



Feature Article

Polymer crystallization process at high supercooling: Crystallization with nodular aggregation region near the glass transition[☆]

Takashi Konishi^{*}, Yoshihisa Miyamoto

Graduate School of Human and Environmental Studies, Kyoto University, Sakyo-ku, Kyoto, 606-8054, Japan



ARTICLE INFO

Keywords:

Polymer crystallization
Aggregation
Crystalline nodular structure
Mesophase
Small angle X-ray scattering
Hierarchical structure

ABSTRACT

Polymer crystallization has been treated as the formation mechanism of lamellae based on secondary nucleation. This treatment has well explained many experimental results especially at a low supercooling. On the other hand, it is also known that some experimental results cannot be fully explained by this model when the degree of supercooling is large. This Feature Article reviews our recent studies on polymer crystallization at a high supercooling. We have revealed the evidence of the crystallization process through the mesophase at a higher supercooling. In addition, we have found the crystallization process with the nodular aggregation near the glass transition temperature. These processes are of great interest for the understanding of polymer crystallization.

1. Introduction

Most of polymers proceed crystallization by quenching from the melt or by heating up from the glass. A typical crystalline morphology for polymers is a thin crystalline plate, so-called lamellae, in the order of nanometer [1,2]. The stacked lamellae constitute a spherulite in the order of micrometer. Some crystalline polymers exhibit globular crystallites, so-called nodules, by deep quenching [3–15]. Other characteristic crystal morphologies include shish-kebab structure formed by shear-induced crystallization [16–20]. The formation mechanisms of these polymer crystalline structures have been investigated for the long time for academic interests but also for industrial applications.

In order to understand the crystallization mechanism of polymers, it is necessary to understand the formation mechanism of the lamellae. The traditional model currently widely used in polymer crystallization has been proposed by Lauritzen and Hoffman as the secondary nucleation and growth process [2,21]. According to the model, the polymer chains (stem), which extend to the thickness of the crystalline lamella, are aligned with the growth surface of the lamella. The Lauritzen–Hoffman's (LH) model has explained many experimental results well when the degree of supercooling is small. On the other hand, it is also known that some experimental results cannot be fully explained by this model when the degree of supercooling is large [15,22–45].

For some polymers crystallized at moderate supercooling, the existence of a crystallization mechanism through a metastable phase has been clarified from the results of the temperature dependences

of crystalline lamellar thickness and growth rate [35,41–47]. This crystallization mechanism is an example of the Ostwald step rule, in which a phase passes through a thermodynamically metastable phase and then transforms to a stable phase.

Recently, it has been found that density fluctuations in several hundred nanometers occur in some polymeric materials during the early stage of crystallization near the glass transition temperature, which is a high supercooling [39,48–51]. We have revealed that the fluctuations come from the aggregation of the nodular crystallites [48–50]. These interesting experimental results suggest that polymer crystallization at a large degree of supercooling is not a simple first-order phase transition from a supercooled liquid. In this Feature Article, we introduce recent studies on polymer crystallization at middle and high supercooling, that involves the formation of nodular aggregates.

2. Theoretical treatment

In this section, we describe two theories used in the Feature Article, the scattering theory for a hierarchical structure [48], and the theory of the nucleation and the growth transition mechanism proposed by Kolmogorov [52], Johnson, Mehl [53] and Avrami [54–56] (KJMA theory).

2.1. SAXS for hierarchical structure

We consider a situation where the entire sample with volume V is filled with N small crystalline globules, called crystalline nodules. The

[☆] Parts of this study are the results of the research project funded by KAKENHI(JP25800236, JP22K03548) and JST CREST(JPMJCR22L4).

^{*} Corresponding author.

E-mail address: konishi.takashi.8c@kyoto-u.ac.jp (T. Konishi).

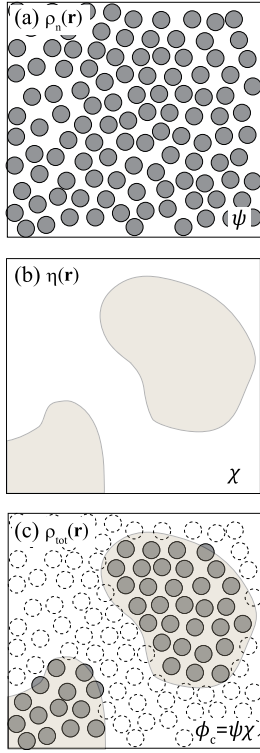


Fig. 1. Illustrations for the density distribution functions of (a) the nodule covering the entire sample, (b) the nodular aggregation region, and (c) the aggregated nodules. Each volume fraction is depicted at the bottom right.

position of the i th nodule is expressed as $\mathbf{r}_i + \mathbf{R}_i$, where \mathbf{r}_i is the center of mass for the i -th nodule, and \mathbf{R}_i is the position from the center of mass for the i -th nodule. Assuming all the nodules have the same shape, we define the density distribution function for the nodular shape as $\rho_p(\mathbf{R}_i)$, which indicates 1 inside the i th nodule and 0 outside that.

The density distribution function of the nodules covering the entire sample, $\rho_n(\mathbf{r})$, can be given by [48]

$$\rho_n(\mathbf{r}) = \rho_a + (\Delta\rho_{ac})\rho_s(\mathbf{r}) * \rho_p(\mathbf{r}) \quad (1)$$

where $*$ indicates convolution, ρ_a and ρ_c indicate the densities of the amorphous and crystal, respectively, $\Delta\rho_{ac} = \rho_c - \rho_a$, $\rho_s(\mathbf{r}) = \sum_i^N \delta(\mathbf{r} - \mathbf{r}_i)$, and $\delta(x)$ is delta function. The volume fraction of the packed nodules in the sample is represented by $\psi = Nv/V$ where v is the volume of each nodule. The illustration of $\rho_n(\mathbf{r})$ is shown in Fig. 1a.

Next, in order to describe the nodular aggregation, we introduce the distribution function of the region of the aggregated nodules, $\eta(\mathbf{r})$, which indicates 1 inside the region and 0 outside that (Fig. 1b). Thus, the position of the nodules in the aggregation regions during the crystallization is given by $\eta(\mathbf{r})\rho_s(\mathbf{r})$. The volume fraction of the aggregation regions is represented by χ . The total distribution function $\rho_{tot}(\mathbf{r})$ can be described as [48]

$$\rho_{tot}(\mathbf{r}) = \rho_a + (\Delta\rho_{ac})\{\eta(\mathbf{r})\rho_s(\mathbf{r})\} * \rho_p(\mathbf{r}). \quad (2)$$

The volume fraction of the nodules in the system corresponds to the crystallinity $\phi_c = \chi\psi$. The illustration of $\rho_{tot}(\mathbf{r})$ is shown in Fig. 1c.

The one-dimensional scattering intensity in the isotropic system, $I_{total}(q)$, can be given by $I_{total}(q) = (1/V)\langle \int \rho_{tot}(\mathbf{r}')\rho_{tot}(\mathbf{r} + \mathbf{r}')e^{-iq\cdot\mathbf{r}'}d\mathbf{r}'d\mathbf{r} \rangle$, where the operator $\langle \rangle$ denotes the ensemble and orientational averages [48]:

$$I_{total}(q) = (\Delta\rho_{ac})^2 \left\{ \chi(1 - \chi)\psi^2 S_\eta(q) + v\psi(1 - \psi)\chi^2 S_n(q) + \frac{v}{(2\pi)^3} \chi(1 - \chi)\psi(1 - \psi)S_\eta(q) * S_n(q) \right\} |\Phi(q)|^2, \quad (3)$$

where $S_\eta(q)$, $S_n(q)$ and $v|\Phi(q)|^2$ are the ensemble- and orientational-averaged Fourier transforms of normalized correlation functions of the distribution functions for $\eta(\mathbf{r})$, $\rho_s(\mathbf{r})$ and $\rho_p(\mathbf{r})$, respectively.

Assuming the size of the aggregation region is sufficiently larger than the nodular size, $S_\eta(q)$ can be regarded as the delta function, $(2\pi)^3\delta(q)$, for $S_n(q)$, and $|\Phi(q)|^2$ can be regarded as unity for $S_\eta(q)$. Thus Eq. (3) can be rewritten as [48]

$$I_{total}(q) = (\Delta\rho_{ac})^2 \left\{ \chi(1 - \chi)\psi^2 S_\eta(q) + \chi\psi(1 - \psi)S_n(q)v|\Phi(q)|^2 \right\}. \quad (4)$$

The term, $(1 - \psi)S_n$, in Eq. (4) is generally expressed as the interparticle interference term, $\mathcal{F}(q)$.

The first and second terms in *r.h.s.* in Eq. (4) indicate the intensities for the nodular aggregates, $I_{aggregate}(q)$, and the nodules in the aggregates, $I_{nodule}(q)$, respectively. When invariant Q is defined by $Q = \int_0^\infty q^2 I(q) dq$, the invariants for $I_{total}(q)$, $I_{aggregate}(q)$, and $I_{nodule}(q)$ for Eq. (4) are respectively given by [48]

$$Q_{total} = 2\pi^2(\Delta\rho_{ac})^2\phi_c(1 - \phi_c) \quad (5)$$

$$Q_{aggregate} = 2\pi^2(\Delta\rho_{ac})^2\chi(1 - \chi)\psi^2 \quad (6)$$

$$Q_{nodule} = 2\pi^2(\Delta\rho_{ac})^2\chi\psi(1 - \psi). \quad (7)$$

These equations satisfy $Q_{total} = Q_{aggregate} + Q_{nodule}$.

2.2. KJMA theory

In this section, we describe the Kolmogorov–Johnson–Mehl–Avrami (KJMA) theory [52–56], which describes the nucleation and growth transition mechanism from a metastable phase to a stable phase in a non-conservative system. The KJMA theory predicts the growth kinetics of the stable phase given by

$$X(t) = 1 - \exp(-Kt^{n_a}) \quad (8)$$

where $X(t)$ is the volume fraction of the stable domains, K is a constant, and n_a is an Avrami exponent. The KJMA theory is actually widely used in the analysis of polymer crystallization. In the following, we derive the equal-time n -body correlation function, $C_n(\mathbf{x}_1, t, \mathbf{x}_2, t, \dots, \mathbf{x}_n, t)$, for the metastable region outside of the stable domains formed by the d -dimensional homogeneous nucleation and growth (HNG) kinetics and inhomogeneous one (IHNG) referring to the Sekimoto's theoretical manner [50,57]. Moreover, we derive time-dependent volume fraction, $X(t)$, and the time-dependent structure factor, $S(q)$, for the stable domains formed by each kinetics.

2.2.1. Homogeneous nucleation and growth process

We describe the equal-time correlation function, $C_n^H(\mathbf{x}_1, t, \mathbf{x}_2, t, \dots, \mathbf{x}_n, t)$, for the situation where the stable domain forms by the HNG kinetics with a nucleation frequency I_n and an isotropic velocity v (Fig. 2a), referring to the Sekimoto's theoretical manner [57].

For $n = 1$, $C_1^H(\mathbf{x}, t)$ is represented as

$$C_1^H(\mathbf{x}, t) = \exp(-\mu_d^H I_n v^d t^{d+1}), \quad (9)$$

where $\mu_{d=1}^H = 1$ and $\mu_{d=2}^H = \mu_{d=3}^H = \pi/3$.

For $n = 2$, $C_2^H(\mathbf{x}, t, \mathbf{x} + \mathbf{r}, t)$ is represented as

$$C_2^H(\mathbf{x}, t, \mathbf{x} + \mathbf{r}, t) = [C_1^H(\mathbf{x}, t)]^2 \exp\left(I_n v^d t^{d+1} \Psi_d^H\left(\frac{|\mathbf{r}|}{2vt}\right)\right), \quad (10)$$

where $\Psi_d^H(y) = 0$ for $y \geq 1$ and for $y < 1$

$$\Psi_{d=1}^H(y) = (1 - y) \quad (11)$$

$$\Psi_{d=2}^H(y) = \frac{2}{3} \left(\arccos y - 2y\sqrt{1 - y^2} + y^2 \ln \frac{\sqrt{1 - y^2}}{y} \right) \quad (12)$$

$$\Psi_{d=3}^H(y) = \frac{\pi}{3} (1 - y)^3 (1 + y). \quad (13)$$

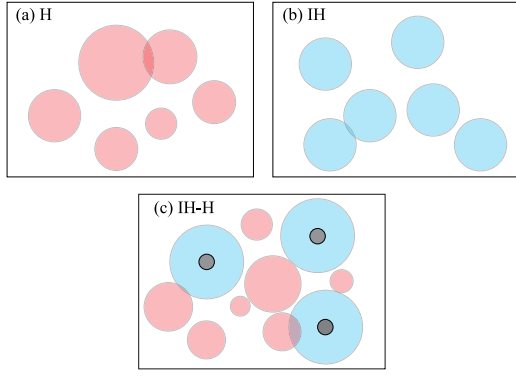


Fig. 2. Illustrations of growth processes of (a) homogeneous nucleation and growth (HNG), (b) inhomogeneous nucleation and growth (IHNG), and (c) inhomogeneous-homogeneous nucleation and growth (IH-HNG).

2.2.2. Inhomogeneous nucleation and growth process

It is considered the equal-time correlation function, $C_n^{\text{IH}}(\mathbf{x}_1, t, \mathbf{x}_2, t, \dots, \mathbf{x}_n, t)$, for the metastable region outside of the stable domains formed by IHNG kinetics with nucleation number density J_n and v (Fig. 2b) [50].

For $n = 1$,

$$C_1^{\text{IH}}(\mathbf{x}, t) = \exp(-\mu_d^{\text{IH}} J_n v^d t^{d+1}) \quad (14)$$

where $\mu_{d=1}^{\text{IH}} = 2$, $\mu_{d=2}^{\text{IH}} = \pi$, and $\mu_{d=3}^{\text{IH}} = 4\pi/3$.

For $n = 2$,

$$C_2^{\text{IH}}(\mathbf{x}, t, \mathbf{x} + \mathbf{r}, t) = [C_1^{\text{IH}}(\mathbf{x}, t)]^2 \exp\left(J_n v^d t^d \Psi_d^{\text{IH}}\left(\frac{|\mathbf{r}|}{2vt}\right)\right) \quad (15)$$

where $\Psi_d^{\text{IH}}(y) = 0$ for $y \geq 1$ and for $y < 1$

$$\Psi_{d=1}^{\text{IH}}(y) = 2(1-y) \quad (16)$$

$$\Psi_{d=2}^{\text{IH}}(y) = 2\left(\arcsin\sqrt{1-y^2} - y^2\sqrt{1-y^2}\right) \quad (17)$$

$$\Psi_{d=3}^{\text{IH}}(y) = \frac{4\pi}{3}(1-y)^2\left(1 + \frac{y}{2}\right). \quad (18)$$

2.2.3. Inhomogeneous-homogeneous nucleation and growth process

Here we consider kinetics of a situation in which the preformed domains with radius Λ growth by IHNG kinetics, and the new domains grow from the rest metastable region in the by HNG kinetics [50]. Here we call the process as the inhomogeneous-homogeneous nucleation and growth process (IH-HNG) shown in Fig. 2c. This situation is not special and can occur during the crystallization process in the presence of the crystal nuclei formed by cooling or of the nucleating agents.

The fictive time t_f is defined as $t_f = \Lambda/v$. The equal-time correlation function, $C_n^{\text{IH-H}}(\mathbf{x}, t)$, for the situation is given by [50]

$$C_1^{\text{IH-H}}(\mathbf{x}, t) = C_1^{\text{H}}(\mathbf{x}, t)C_1^{\text{IH}}(\mathbf{x}, t') \quad (19)$$

and

$$C_2^{\text{IH-H}}(\mathbf{x}, t, \mathbf{x} + \mathbf{r}, t) = C_2^{\text{H}}(\mathbf{x}, t, \mathbf{x} + \mathbf{r}, t)C_2^{\text{IH}}(\mathbf{x}, t', \mathbf{x} + \mathbf{r}, t') \quad (20)$$

where $t' = t + t_f$.

2.2.4. Volume fraction and scattering function for stable domains

The time-dependent volume fraction for the stable domain formed by the HNG, IHNG or IH-HNG kinetics is given by [50,57]

$$X(t) = 1 - C_1^k(\mathbf{x}, t). \quad (k = \text{H, IH, IH-H}) \quad (21)$$

The derived equation is same as Eq. (8).

The scattering function for the metastable region, $S_{\text{meta}}^k(\mathbf{q}, t)$, in the HNG system can be given by [57]

$$S_{\text{meta}}^k(\mathbf{q}, t) = \int d\mathbf{r} e^{i\mathbf{q}\cdot\mathbf{r}} C_2^k(\mathbf{x}, t, \mathbf{x} + \mathbf{r}, t) \quad (22)$$

$$= (2\pi)^d [C_1^k(\mathbf{x}, t)]^2 \delta(\mathbf{q}) + \tilde{S}^k(\mathbf{q}, t) \quad (23)$$

where

$$\tilde{S}^k(\mathbf{q}, t) = \int d\mathbf{r} e^{i\mathbf{q}\cdot\mathbf{r}} \{C_2^k(\mathbf{x}, t, \mathbf{x} + \mathbf{r}, t) - [C_1^k(\mathbf{x}, t)]^2\}. \quad (24)$$

Considering the Babinet's principle, the structure factor for stable domains, $S^k(\mathbf{q}, t)$, can be given by

$$S^k(\mathbf{q}, t) = (2\pi)^d [1 - C_1^k(\mathbf{x}, t)]^2 \delta(\mathbf{q}) + \tilde{S}^k(\mathbf{q}, t). \quad (25)$$

For example, isotropic $S^k(\mathbf{q}, t)$ for the three dimensional HNG system, $S_{d=3}^{\text{H}}(q, t)$, can be written as [49]

$$S_{d=3}^{\text{H}}(q, t) = (2\pi)^3 [X_{d=3}^{\text{H}}(t)]^2 \delta(q) + \tilde{S}_{d=3}^{\text{H}}(q, t), \quad (26)$$

where

$$X_{d=3}^{\text{H}}(t) = 1 - \exp\left(-\frac{\pi}{3} J_n v^3 t^4\right) \quad (27)$$

and

$$\begin{aligned} \tilde{S}_{d=3}^{\text{H}}(q, t) &= 4\pi \exp\left(-\frac{2\pi}{3} J_n v^3 t^4\right) (2vt)^3 \\ &\times \int_0^1 dy y^2 \frac{\sin(2vtyq)}{2vtyq} \{\exp[J_n v^3 t^4 \Psi_3^{\text{H}}(y)] - 1\}. \end{aligned} \quad (28)$$

In addition, $S^k(\mathbf{q}, t)$ for the three-dimensional IH-HNG system, $S_{d=3}^{\text{IH-H}}(q, t)$, can be also written as [50]

$$S_{d=3}^{\text{IH-H}}(q, t) = (2\pi)^3 [X_{d=3}^{\text{IH-H}}(t)]^2 \delta(q) + \tilde{S}_{d=3}^{\text{IH-H}}(q, t), \quad (29)$$

where

$$X_{d=3}^{\text{IH-H}}(t) = 1 - \exp\left(-\frac{\pi}{3} J_n v^3 t^4 - \frac{4\pi}{3} J_n v^3 t^3\right) \quad (30)$$

and

$$\begin{aligned} \tilde{S}_{d=3}^{\text{IH-H}}(q, t) &= \\ &4\pi [1 - X_{d=3}^{\text{IH-H}}(t)]^2 (2vt)^3 \left[\int_0^1 dy y^2 \frac{\sin(2vtyq)}{2vtyq} \right. \\ &\times \left\{ \exp\left[J_n v^3 t^4 \Psi_3^{\text{IH}}(y) + J_n v^3 t^3 \Psi_3^{\text{IH}}\left(\frac{t}{t'} y\right)\right] - 1 \right\} \\ &\left. + \int_1^{t'/t} dy y^2 \frac{\sin(2vtyq)}{2vtyq} \{\exp[J_n v^3 t^3 \Psi_3^{\text{IH}}\left(\frac{t}{t'} y\right)] - 1\} \right]. \end{aligned} \quad (31)$$

3. Polymer crystallization at low or middle supercooling: Polymer crystallization through mesophase

Micrometer scale morphologies of polymers crystallized at a very low supercooling is hedrite or axillite [1]. When the degree of supercooling increases, the morphology changes to spherulite. Spherulites are observed in a wide temperature range. These morphologies consist of the stacked crystalline lamellae in nano-meter size. The ordinary polymer crystallization mechanism can be, therefore, understood as the formation mechanism of the lamella.

The melting temperature, T_m , of the crystalline lamella depends on the lamellar thickness, ℓ , because of the surface free energy between the amorphous and crystal. The relation between ℓ and T_m are given by [1]

$$T_m = T_m^0 - \frac{2\zeta_e T_m^0}{\Delta H_m \ell} \quad (32)$$

where T_m^0 is the equilibrium melting temperature, which is the melting temperature of the infinitely large crystal, ζ_e is the folding surface free energy, and ΔH_m is the enthalpy difference between crystal and amorphous. This relation is well-known as the Gibbs-Thomson relation.

The thickness, ℓ_c , of lamellae formed at the crystallization temperature, T_c , is empirically known as [2]

$$\ell_c = \frac{2\zeta_e T_m^0}{\Delta H_m (T_m^0 - T_c)} + \delta \ell \quad (33)$$

where $\delta\ell$ is the constant excess thickness.

The growth mechanism of the spherulite can be regarded as that of the lamella and has been treated as the secondary nucleation process on the growth face of the formed crystalline lamella. The growth rate, u , of lamella depends on the size of the secondary nucleus, and the secondary nucleus thickens by passing through the critical nucleus [58–61]. The growth rate of spherulite, u , at T_c is given by [2]

$$u = u_0 \beta \exp \left[-\frac{K_G}{T_c(T_m^0 - T_c)} \right]. \quad (34)$$

where u_0 is a constant, T_m^0 is the equilibrium melting temperature, and β is the Vogel–Fulcher–Tammann type diffusion term, given by $\beta = \exp(-\frac{U}{R(T_c - T_V)})$, U is a constant, R is the ideal gas constant, and T_V is the Vogel temperature. K_G is given by

$$K_G = \frac{n_R b \zeta_e \zeta_s T_m^0}{k_B \Delta H} \quad (35)$$

where ζ_s is the lateral surface free energy of the stem, k_B is the Boltzmann constant, and b is the thickness of the stem added on the substrate [2]. In Eq. (35), the value of n_R is $n_R = 4$ for the single nucleation growth (Regime I) or $n_R = 2$ for the multiple nucleation growth (Regime II) [2]. The temperature dependence of u follows Eq. (34). The diffusion term takes a smaller value as it approaches T_g , and the exponential term takes a smaller value as it approaches T_m^0 . Therefore u has a maximum value at a certain temperature between T_g and T_m .

On the other hand, Keller and co-workers have proposed the crystallization mechanism through the transient mesophase from the experimental results of the single crystal of polyethylene (PE) formed under high pressure and high temperature [45,62]. Strobl and coworkers also have proposed the similar crystallization model from the temperature dependences of ℓ and u [35,46,47].

According to these models, the transient mesophase forms at the growth front of lamella below a temperature, T_X , and transforms into the thermodynamically stable crystal by thickening. We explain the crystallization model through the mesophase based on the Keller's treatment [45] as follows [41–43].

First, the transitions between liquid and crystal, LC, between mesophase and liquid, LM, and between mesophase and crystal, MC, are considered. The transition temperatures of LC, LM, and MC are written as T_{LC} , T_{LM} , and T_{MC} , respectively, where $T_{LC} = T_m$. Since these temperature depends on ℓ , the ℓ -dependent transition temperatures are given by [45]

$$T_\alpha = T_\alpha^0 - \frac{2\zeta_{e,\alpha} T_\alpha^0}{\Delta H_\alpha \ell} \quad (\alpha = LC, LM, MC) \quad (36)$$

where ΔH_α and T_α^0 are the enthalpy difference between two phases and the equilibrium transition temperature of each phase. $\zeta_{e,LC}$ and $\zeta_{e,LM}$ are the folding surface free energies of the crystal and mesophase, respectively, and $\zeta_{e,MC}$ is defined as $\zeta_{e,MC} = \zeta_{e,LC} - \zeta_{e,LM}$.

The ℓ - T_α diagram based on Eq. (36) is shown in Fig. 3. The three transition lines intersect at the triple point, T_X and ℓ_X . When the polymer crystallized at $T_c > T_X$, the crystalline lamella directly forms and thickens to ℓ_c (see case I in Fig. 3). This process is the classic process that has been considered for a long time, and the growth rate is described by Eq. (34).

On the other hand, when $T_c < T_X$, the mesomorphic stem firstly forms at the growth front of lamella, thickens to a thickness on the MC transition line, transforms into the crystalline stem, and slightly thickens to ℓ_c given as [42]

$$\ell_c = \frac{2\zeta_{e,MC} T_{MC}^0}{\Delta H_{MC}(T_{MC}^0 - T_c)} + \delta\ell, \quad (37)$$

(see case II in Fig. 3). Since the growth rate at $T_c < T_X$ has been considered as that of the mesophase, the growth rate u becomes [43,45]

$$u = u_0 \beta \exp \left[-\frac{K_{G,LM}}{T_c(T_{LM}^0 - T_c)} \right], \quad (38)$$

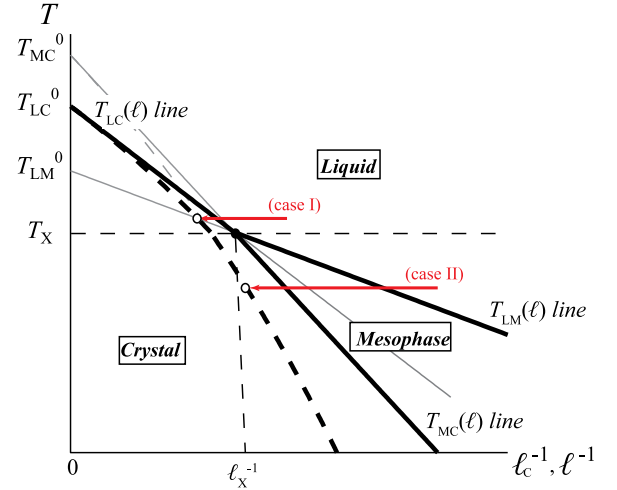


Fig. 3. Illustrations for the ℓ^{-1} - T_α phase diagram based on Eq. (36). Thick solid lines indicate the ℓ -dependences of the transition temperatures of T_{LC} , T_{LM} , and T_{MC} in Eq. (36). Thick broken line indicates the T_c -dependences of ℓ_c obtained by Eqs. (33) and (37).

where

$$K_{G,LM} = \frac{2b\zeta_{e,LM}\zeta_{s,LM}T_{LM}^0}{k_B\Delta H_{LM}}, \quad (39)$$

and $\zeta_{s,LM}$ is the lateral surface free energy of the mesomorphic stem.

The existence of the crystallization process through the mesophase has been confirmed in some polymers, PE [45,62,63], syndiotactic polypropylene (sPP) [35,46,47,64], poly(ϵ -caprolactone) [65–67], isotactic polystyrene [68], poly(L-lactide) [69], poly(buthylene terephthalate) (PBT) [7,41–44], and poly(buthylene naphthalate) (PBN) [70,71]. Among them, the T -dependences of ℓ and u for PBT [42,43] is shown in Fig. 4. The results of PBT directly show the existence of T_X in both the T -dependences of ℓ and u .

The transient mesophase of PBT at the growth front at $T_c < T_X$ may be the smectic phase formed near its T_g [72]. The smectic phase of PBT is formed when stretched below T_g , and it immediately transforms into crystals with annealing above T_g [72]. The temperature dependence of crystalline size in PBT crystallized near T_g can be also explained by the crystallization through the mesophase [7].

Poly(buthylene naphthalate) (PBN) also forms the smectic phase near its T_g [70]. The amorphous-smectic-crystal transition process is directly observed during rapid deep quenching process in PBN [71]. These results might support a transient mesophase formed at the growth front is a smectic phase.

As described above, the crystallization process through the mesophase appears as the degree of supercooling increases. This process can be treated as the lamella formation process based on the secondary nucleation mechanism.

4. Polymer crystallization near the glass transition temperature

As mentioned in the Section 3, the lamellar structure forms by the secondary nucleation growth even in the crystallization process through the mesophase. However, in the crystallization process near T_g , there are phenomena that cannot be explained by the lamella formation process based on the secondary nucleation mechanism. Some polymers crystallized near their T_g at high supercooling exhibit the nodular crystalline morphology rather than the lamella [3–15], and the density fluctuations are suggested or reported during the early stage of polymer crystallization [22–26,28–34,36,39,40,51]. The origins of the nodular crystal formation and the density fluctuations have not been sufficiently understood.

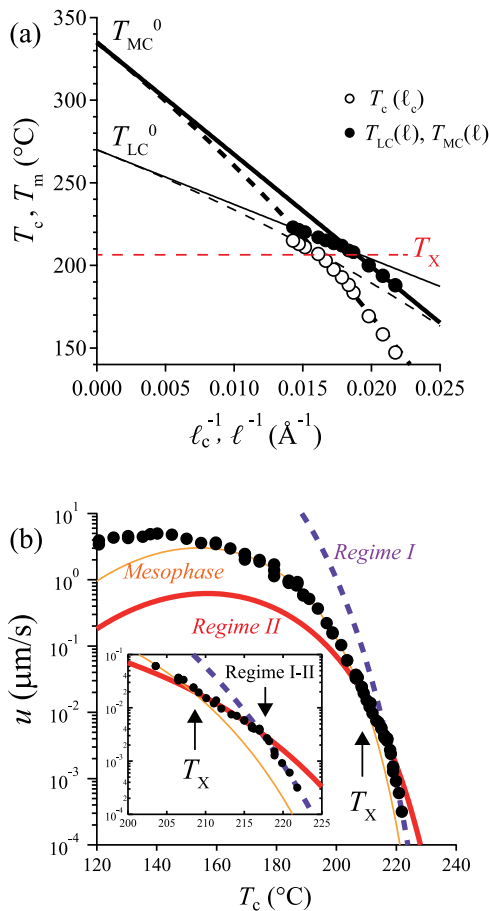


Fig. 4. T -dependences of (a) the lamellar thicknesses, ℓ and ℓ_c [42], and (b) the growth rate, u [43], for PBT. In (a), open circles indicate $T_c(\ell_c)$ [42], filled circles indicate $T_{LC}(\ell)$ and $T_{MC}(\ell)$ [42], and the thick and thin solid lines indicate MC and LC transition lines, and the thick and thin broken curves indicate the T_c -dependences of ℓ_c with Eqs. (33) and (37), respectively.

Recently the density fluctuations have been detected by the small angle X-ray scattering (SAXS) during the early stage of crystallization near T_g for poly(trimethylene terephthalate) (PTT) [39,48,49] and syndiotactic polypropylene (sPP) [50] as shown in Fig. 5. T_g and T_m^0 for PTT are $T_g = 45$ °C and $T_m^0 = 290$ °C [44], and for sPP ($M_w = 174,000$, $rrrr = 0.85$) are $T_g = -3.5$ °C and $T_m^0 = 182$ °C [73].

The crystalline morphologies of PTT [39] and sPP [8,9] crystallized near T_g have been observed by transmission electron microscope (TEM) and atomic force microscopy (AFM), respectively. Both of the morphologies are the nodules in tens nm rather than the lamellae.

We have clarified that the origin of the density fluctuations near T_g is the correlation between aggregates of the nodules and have proposed the crystallization process with the nodular aggregation near T_g [48–50]. These results might be a key of the polymer crystallization at high supercooling. In this section, we review these research results for PTT and sPP [48–50].

We have investigated the isothermal crystallization process of PTT at T_c near T_g from its molten state by simultaneous small angle X-ray scattering (SAXS) and wide angle x-ray diffraction (WAXD). Fig. 6 shows the WAXD profiles of isothermal crystallization processes at $T_c = 60$ °C for PTT and at $T_c = 5$ °C for sPP. The WAXD profiles in Fig. 6a for PTT show the only amorphous halo just after quenching. The Bragg peaks of triclinic crystalline structure [74] increase and the amorphous halo decreases with time. Crystallinity ϕ_c^W can be calculated from the WAXD profiles $I^W(q)$ by the equation $I^W(q) = (1 - \phi_c^W)I_{\text{halo}}^W(q) + \phi_c^W \Sigma I_{\text{Bragg}}^W(q)$, where $I_{\text{halo}}^W(q)$ is the amorphous halo

for the complete amorphous and $\Sigma I_{\text{Bragg}}^W(q)$ is the sum of the Bragg peaks for the complete crystal. Fig. 7 shows t_c -dependent ϕ_c^W of PTT crystallized at $T_c = 60$ °C.

The WAXD profiles in Fig. 6b for sPP show an amorphous halo and very small Bragg peaks just after quenching. The Bragg peaks at $t_c = 0$ sec originate from the nucleation during quenching. The WAXD profiles for sPP can be expressed by the sum of amorphous, crystalline Form I, and mesophase. It is noted that the mesophase in sPP detected by WAXD is the different from the transient mesophase formed at the growth front discussed in Section 3. The chain conformation in the mesophase of sPP is trans-planar [75–84] and that in Form I is $s(2/1)2$ [85–87]. The component ratio of Form I and mesophase does not change with t_c [50]. This result indicates that Form I and the mesophase simultaneously form during the isothermal crystallization. Here, the sum of the components of Form I and the mesophase is written as ϕ_c^W . Fig. 7 shows t_c -dependent ϕ_c^W of sPP crystallized at $T_c = 5$ °C.

Fig. 5 shows the SAXS profiles $I^S(q)$ of the isothermal crystallization process at $T_c = 60$ °C for PTT [49] and at $T_c = 5$ °C for sPP [50]. Since $I^S(q)$ for both PTT and sPP shows different behaviors in the low- and high- q regions, $I^S(q)$ can be given by $I^S(q) = I_L(q) + I_H(q)$, where $I_L(q)$ and $I_H(q)$ represent $I^S(q)$ at $q < 0.02$ Å⁻¹ and $q > 0.02$ Å⁻¹, respectively.

For PTT, the intensity $I_L(q)$ decreases with q , and increases with t_c until 260 s and then decreases after 260 s. On the other hand, $I_H(q)$ has a peak against q , and monotonically increases with t_c . Similar to the behavior of PTT, $I_L(q)$ in sPP increases and then decreases with t_c , and $I_H(q)$ monotonically increases with t_c . As mentioned above, the morphologies of PTT and sPP are the nodules, and thus the peak of $I_H(q)$ corresponds to a periodic correlation among the nodules. $I_L(q)$ and $I_H(q)$ comes from the correlation between the nodular aggregates and that between the nodules in each aggregate, respectively [48].

According to the discussion in Section 2.1, $I^S(q)$, $I_L(q)$, and $I_H(q)$ corresponds with $I_{\text{total}}(q)$, $I_{\text{aggregate}}(q)$, and $I_{\text{nodule}}(q)$, respectively. Chuang and coworker have analyzed the $I_H(q)$ behavior during the crystallization [39]. According to their analysis, $I_H(q)$ can be fitted well by applying the Percus–Yevick approximation [88] of the hard spheres model to $\mathcal{F}(q)$ and the ellipsoidal shape to $|\Phi(q)|^2$ in Eq. (4). The fitting result leads that the distribution of the crystalline nodules in the aggregation region is discrete and random, and is consistent with the TEM image.

Furthermore, the formation kinetics of the aggregation region during the crystallization can be discussed in detail using the invariants Q as mentioned in Section 2.1. The t_c -dependences of Q for $I^S(q)$, $I_L(q)$ and $I_H(q)$ correspond with Q_{total} , $Q_{\text{aggregate}}$, and Q_{nodule} , respectively. These Q behaviors give the volume fractions of the aggregates of crystalline nodules, χ , that of the nodules in the aggregation region, ψ , and crystallinity ϕ_c using Eqs. (5)–(7). Assuming constant ψ , the values of χ , χ^Q , ψ , ψ^Q , and ϕ_c , ϕ_c^Q , can be calculated from the invariants of $I_L(q)$ and $I_H(q)$ [48]. t_c -dependent χ^Q , ψ^Q , and ϕ_c^Q for PTT and sPP are shown in Fig. 7. The t_c -dependence of ϕ_c^Q quantitatively agrees with that of ϕ_c^W .

We focus on the kinetics of the time evolution of χ in Fig. 7, and discuss the kinetics by the KJMA theory discussed in Section 2.2. The time evolution of χ for PTT can be expressed by Eq. (8) with $n_a = 4$, that is, the kinetics of the nodular aggregate formation is three-dimensional HNG. This fitting result gives the value of $I_n v^3$ at T_c for PTT using Eq. (27). On the other hand, the χ for sPP is expressed by Eq. (8) with $n_a = 2.1$. The reason of the low value of n_a for sPP is the nucleation during quenching as discussed in the WAXD result. The multifaceted aggregates with a diameter of several tens of nanometers in sPP quenched just above T_g have been found by AFM [8,9]. In order to remove the influence of this nucleation, calculations considering the IH-HNG process in Section 2.2.3 are necessary [50]. The t_c -dependence of χ for sPP can be fitted by Eq. (30), and the fitting result gives the values of $I_n v^3$, $J_n v^3$, and t_f at T_c for sPP. These fitting results shows that

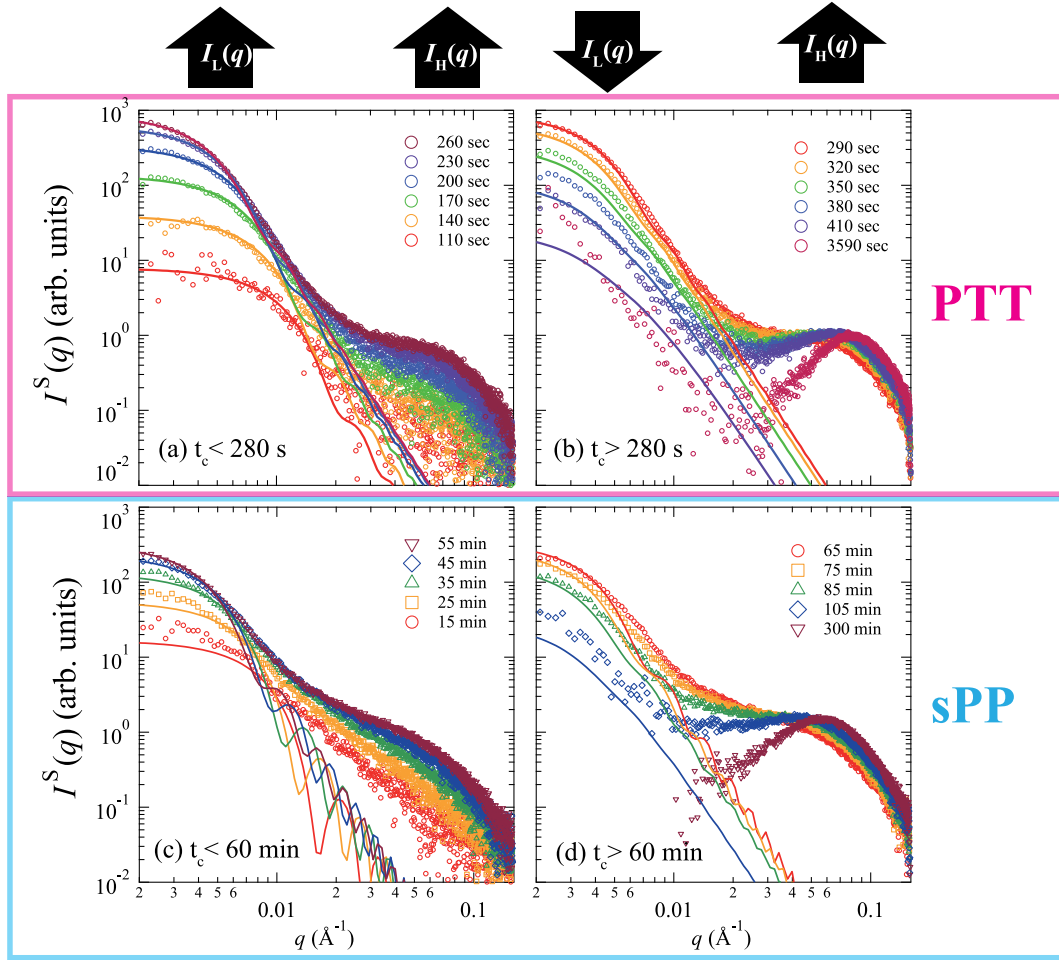


Fig. 5. SAXS profiles $I^S(q)$ as a function of t_c for PTT crystallized at 60 °C from the melt (a) until and (b) after 280 sec [49], and for sPP crystallized at 5 °C from the melt (a) until and (b) after 60 min [50]. The solid curves in (a) and (b) are the theoretical curves obtained using $S_{d=3}^H(q)$ with $\nu = 2.3 \text{ \AA s}^{-1}$, and $I_n = 1.26 \times 10^{-11} \text{ \AA}^{-3} \text{ s}^{-1}$. The solid curves in (c) and (d) are the theoretical curves obtained using $S_{d=3}^{IH-H}(q)$ with $t_f = 24.1 \text{ min}$, $\nu = 7.1 \text{ \AA min}^{-1}$, and $I_n = 1.22 \times 10^{-11} \text{ \AA}^{-3} \text{ min}^{-1}$, and $J_n = 1.00 \times 10^{-9} \text{ \AA}^{-3}$.

the formation kinetics of the nodular aggregates is three-dimensional HNG.

In order to examine the validity of these results, we also discuss the SAXS profiles. The fact that the aggregate formation is of HNG type allows a deeper analysis of t_c -dependent $I_L(q)$, which is the correlation of the nodular aggregation regions. $I_L(q)$ corresponds with the first term in Eq. (4), $I_{\text{aggregate}}(q)$, and does with $\bar{S}_{d=3}^H(q, t)$ in Eq. (28) as discussed in Section 2.2. The fitting of $\bar{S}_{d=3}^H(q, t)$ to $I_L(q)$ for PTT, shown in Figs. 5a and 5b, can obtain the aggregate growth rate ν and nucleation frequency I_n . Fig. 8 shows the temperature dependences of ν and I_n obtained from SAXS results performed at various crystallization temperatures T_c for PTT.

On the other hand, $I_L(q)$ for sPP also can be fitted using $\bar{S}_{d=3}^{IH-H}(q, t)$ for IH-HNG (Eq. (31)) in Figs. 5c and 5d. Fig. 8 also shows ν for sPP at $T_c = 5 \text{ }^\circ\text{C}$. The values of $\nu = 7.1 \text{ \AA min}^{-1}$ and $t_f = 24.1 \text{ min}$ give the preformed aggregate size $\Lambda = 171 \text{ \AA}$. The value of Λ is of the same order as the size of the multifaceted aggregate reported by the other groups [8,9]. This correspondence supports the validity of the application of the IH-HNG process to sPP.

These values of ν and I_n are compared with the spherulite growth rate u obtained by optical microscopy at high temperatures in Fig. 8. The secondary nucleation type spherulitic growth rate, u , for polymer is well written by Eq. (34) with $n_R = 2$. The fitting growth rate curve in Fig. 8 shows that the T_c -dependence of ν is a natural extrapolation of that of u to the high supercooling region.

The homogeneous nucleation rate, I_n , for the chain-folded crystalline lamella is given as [2].

$$I_n = I_{n0} \beta \exp \left[-\frac{K_I}{T_c(T_m^0 - T_c)^2} \right] \quad (40)$$

where

$$K_I = \frac{32\zeta_e\zeta_s^2(T_m^0)^2}{k_B\Delta H_m^2} \quad (41)$$

The relation between ζ_s and ΔH is given as the Thomas–Staveley (TS) relation [89,90], $\zeta_s = \alpha_{TS} \sqrt{ab\Delta H_m}$, where α_{TS} is constant depending on material properties and a is the width of the stem. Assuming $a \cong b$, the combination among K_G with $n_R = 2$ for Regime II, K_I , and the TS relation leads [49]

$$\frac{K_I}{K_G} = 16\alpha_{TS} T_m^0. \quad (42)$$

The value of α_{TS} is estimated as 0.3–0.4 for ordinary organic materials [89] and 0.1–0.3 for polymers [43,90]. Thus the T_c -dependence of I_n for PTT in Fig. 8 also can be represented by the parameters estimated for the lamellar growth u with $\alpha_{TS} = 0.27$ [49]. The results of ν , u and I_n show that the nucleation rate and growth rate of the aggregation region composed of the discretely located nodules can be described using the parameter estimated for the ordinary lamellar growth.

We summarize the experimental results and discussion in Sections 3 and 4. The lamellar growth through the transient mesophase can be

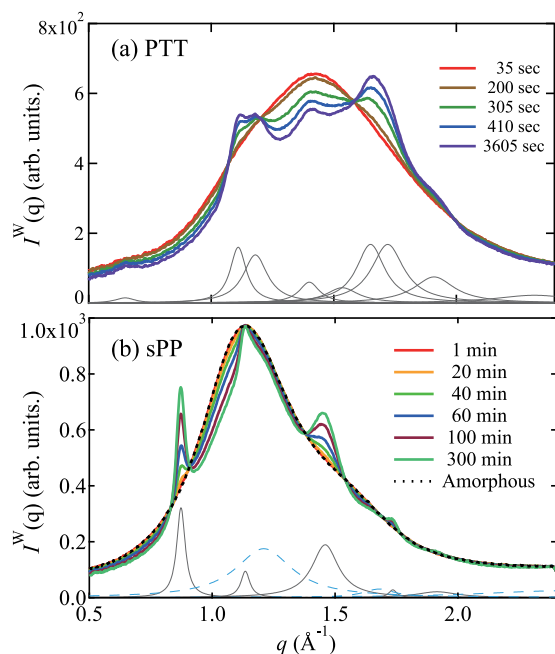


Fig. 6. WAXD profiles $I^W(q)$ as a function of q (a) for PTT [49] crystallized at 60 °C from the melt and (b) for sPP [50] crystallized at 5 °C from the melt. Thick solid curves are experimentally obtained data. A thick dotted curve is the estimated amorphous halo. Thin solid curves in (a) and (b) are the Bragg peaks corresponding to the crystals of PTT and sPP, respectively. Thin broken curves in (b) are the mesophase intensities of sPP.

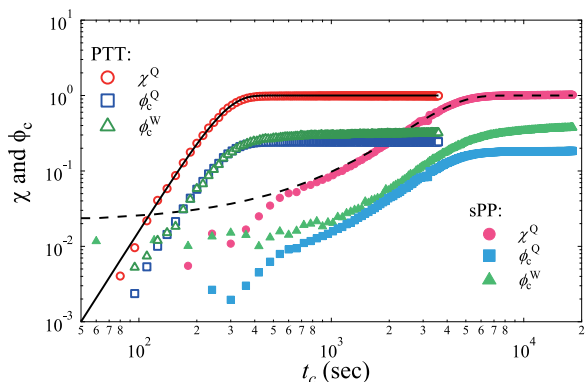


Fig. 7. t_c -dependent crystallinity, ϕ_c , and volume fraction of aggregation region, χ , for PTT and sPP. Open circles, squares, and triangles indicate χ^Q , ϕ_c^Q , and ϕ_c^W , respectively, in PTT [49]. Filled circles, squares, and triangles indicate χ^Q , ϕ_c^Q , and ϕ_c^W , respectively, in sPP [50].

treated as secondary nucleation as mentioned in Section 3. On the other hand, as shown in Section 4, the crystallization process with the nodular aggregation proceeds near T_g , and the kinetics of the crystallization process with the nodular aggregation is similar to that of the lamellar crystallization at the low and middle supercooling. These experimental results might indicate that the transient mesophase formed in lamellar formation process is not directly related to the nodule formation process. These discussions provide a following possible scenario for polymer crystallization. The precursor or embryo forms in front of the growth face of the aggregation region or the lamella. The precursor is incorporated and transforms into a part of the crystalline lamella well above T_g , while it transforms into the crystalline nodule without transforming into the lamellae near T_g .

The homogeneous nucleation process near T_g has been detected for many polymers by fast differential scanning calorimetry (fast-DSC) [15].

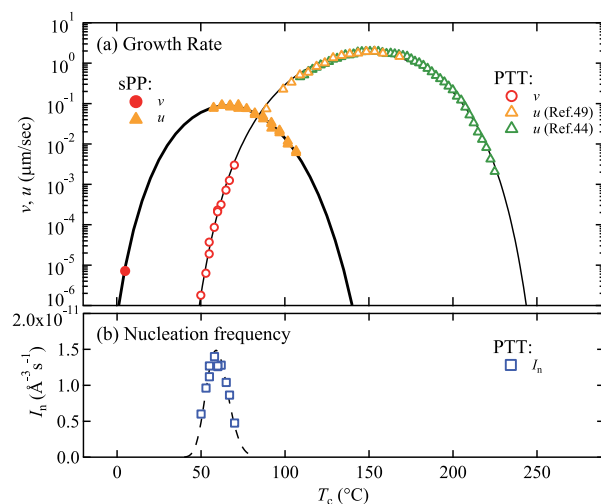


Fig. 8. T_c -dependences of (a) the growth rates of the nodular aggregates, v , and of the spherulites u , and (b) the nucleation frequency of the nodular aggregates, I_n , in PTT and sPP. Open circles, squares, and triangles indicate v [49], I_n [49], and u [44,49] in PTT, respectively. Filled circles and triangles indicate v and u in sPP [50], respectively. The thin and thick solid curves in (a) indicate the v curves calculated using Eq. (34) for PTT and sPP, respectively. The thin broken curve in (b) indicates the I_n -curves calculated using Eqs. (40) and (42).

Our results strongly suggest that the homogeneous nucleation detected by fast-DSC comes from the formation of the aggregation regions of the nodules. Recently the relation between the morphologies and the crystallization kinetics in PBT has been investigated by fast-DSC and AFM [91]. These results show that the HNG occurs near T_g and that the morphology formed during this process is nodule. Furthermore it has been concluded that the nodular formation near T_g is due to the rigid-amorphous surrounding the nodules [91]. The strong relation between morphology of the single crystal and the diffusion of amorphous surrounding it has been also reported [92–94].

Some interesting observations have also been reported regarding the lamellar morphology formed at middle supercooling. The lamellae composed of the crystalline nodules (small globules) have been observed by electron microscopy [64,95,96]. Strobl has proposed the model that the lamellae form with attaching the small globules at the growth front through the mesophase [35]. Miyoshi and coworkers [37,38] have reported using nuclear magnetic resonance (NMR) techniques that there are chain foldings even in the nodules of isotactic polypropylene and that the NMR results are direct evidence of the cooperative coarsening of the nodules.

These results are consistent with our scenario. Muthukumar’s model explains the early stage of nucleation by precursor “baby nuclei” followed by a cooperative coarsening of these multiple nuclei on the basis of the entropic effect of the polymer chain between baby nuclei by theoretical and simulation methods [30–32]. Our experimental results indicate that the nodules easily form around the already formed nodular aggregates. Understanding of the formation mechanism of nodular aggregates might require the consideration of the entropic effects of polymer chains.

It is unique that the nucleation and growth mechanism of the aggregate of the “discretely” located nodules and that of the spherulite are the same since the general crystallization models are based on the attachment of molecules to the growth front. Complete understanding of these results require a unified crystal growth mechanism which can treat both nodular aggregation and lamellar growth. The two-step crystallization process with forming precursors has been discussed in the other system [97–107]. It is also important to investigate the relation between our results and the two-step crystallization process.

5. Summary

In this Feature Article, we have summarized recent experimental results of polymer crystallization at middle and high supercooling. The results clarify following findings. The crystallization through the transient mesophase proceeds at middle supercooling, and its mechanism can be explained by the lamella formation mechanism extended by the Ostwald step rule. The crystallization process with the nodular aggregation proceeds near T_g . The growth rate of the aggregates is a natural extrapolation of that of lamella to the high supercooling region. These findings are of great interest for the understanding of polymer crystallization.

CRedit authorship contribution statement

Takashi Konishi: Writing – original draft, Visualization, Validation, Supervision, Resources, Project administration, Methodology, Investigation, Funding acquisition, Formal analysis, Data curation, Conceptualization. **Yoshihisa Miyamoto:** Writing – review & editing, Validation, Data curation.

Declaration of competing interest

The authors declare that they have no known competing financial interests or personal relationships that could have appeared to influence the work reported in this paper.

Data availability

Data will be made available on request.

Acknowledgments

Parts of this work are the results of the research project funded by KAKENHI (JP25800236, JP22K03548) and JST CREST (JPMJCR22L4).

References

- [1] G.R. Strobl, *The Physics of Polymers*, Springer, 1997.
- [2] J.D. Hoffman, G.T. Davis, J.I. Lauritzen Jr., The rate of crystallization of linear polymers with chain folding, in: *Treatise on Solid State Chemistry: Volume 3 Crystalline and Noncrystalline Solids*, Springer, 1976, pp. 497–614.
- [3] C. Hsu, P. Geil, Morphology-structure-property relationships in ultraquenched poly (vinylidene fluoride), *J. Appl. Phys.* 56 (9) (1984) 2404–2411.
- [4] H. Miyaji, P. Geil, Annealing of nodular linear polyethylene crystallized from the glass, *Polymer* 22 (5) (1981) 701–703.
- [5] C. Hsu, P. Geil, H. Miyaji, K. Asai, Structure and properties of polypropylene crystallized from the glassy state, *J. Polym. Sci. B: Polym. Phys.* 24 (10) (1986) 2379–2401.
- [6] T. Konishi, K. Nishida, T. Kanaya, Crystallization of isotactic polypropylene from prequenched mesomorphic phase, *Macromolecules* 39 (23) (2006) 8035–8040.
- [7] T. Konishi, Y. Miyamoto, Crystallization of poly (butylene terephthalate) from the glass, *Macromolecules* 43 (1) (2010) 375–383.
- [8] R. Pucciariello, V. Villani, A. Cascone, L. Guadagno, V. Vittoria, Crystallization kinetics and morphology of the mesomorphic form of syndiotactic polypropylene, *J. Polym. Sci. B: Polym. Phys.* 45 (8) (2007) 936–944.
- [9] O. Ruiz de Ballesteros, F. De Stefano, F. Auriemma, R. Di Girolamo, M. Scoti, C. De Rosa, Evidence of nodular morphology in syndiotactic polypropylene from the quenched state, *Macromolecules* 54 (16) (2021) 7540–7551.
- [10] D. Gezovich, P. Geil, Morphology of quenched polypropylene, *Polym. Eng. Sci.* 8 (3) (1968) 202–209.
- [11] R. Androsch, A.M. Rhoades, I. Stolte, C. Schick, Density of heterogeneous and homogeneous crystal nuclei in poly (butylene terephthalate), *Eur. Polym. J.* 66 (2015) 180–189.
- [12] D. Mileva, R. Androsch, E. Zhuravlev, C. Schick, Morphology of mesophase and crystals of polyamide 6 prepared in a fast scanning chip calorimeter, *Polymer* 53 (18) (2012) 3994–4001.
- [13] A.M. Gohn, A.M. Rhoades, N. Wonderling, T. Tighe, R. Androsch, The effect of supercooling of the melt on the semicrystalline morphology of PA 66, *Thermochim. Acta* 655 (2017) 313–318.
- [14] K. Jariyavidyanont, C. Schick, R. Androsch, Nucleation-controlled dual semicrystalline morphology of polyamide 11, *Polym. Int.* 68 (2) (2019) 263–270.
- [15] C. Schick, R. Androsch, J. Schmelzer, Homogeneous crystal nucleation in polymers, *J. Phys.: Condens. Matter* 29 (45) (2017) 453002.
- [16] J. Smook, A.J. Pennings, Elastic flow instabilities and shish-kebab formation during gel-spinning of ultra-high molecular weight polyethylene, *J. Mater. Sci.* 19 (1984) 31–43.
- [17] R.H. Somani, L. Yang, L. Zhu, B.S. Hsiao, Flow-induced shish-kebab precursor structures in entangled polymer melts, *Polymer* 46 (20) (2005) 8587–8623.
- [18] S. Kimata, T. Sakurai, Y. Nozue, T. Kasahara, N. Yamaguchi, T. Karino, M. Shibayama, J.A. Kornfield, Molecular basis of the shish-kebab morphology in polymer crystallization, *Science* 316 (5827) (2007) 1014–1017.
- [19] B.S. Hsiao, L. Yang, R.H. Somani, C.A. Avila-Orta, L. Zhu, Unexpected shish-kebab structure in a sheared polyethylene melt, *Phys. Rev. Lett.* 94 (11) (2005) 117802.
- [20] T. Kanaya, G. Matsuba, Y. Ogino, K. Nishida, H.M. Shimizu, T. Shinohara, T. Oku, J. Suzuki, T. Otomo, Hierarchic structure of shish-kebab by neutron scattering in a wide Q range, *Macromolecules* 40 (10) (2007) 3650–3654.
- [21] J.I. Lauritzen Jr., J.D. Hoffman, Theory of formation of polymer crystals with folded chains in dilute solution, *J. Res. Natl. Bureau Stand. Sect. A, Phys. Chem.* 64 (1) (1960) 73.
- [22] G. Allegra, Chain folding and polymer crystallization: A statistical-mechanical approach, *J. Chem. Phys.* 66 (12) (1977) 5453–5463.
- [23] K. Fukao, Y. Miyamoto, Dynamical transition and crystallization of polymers, *Phys. Rev. Lett.* 79 (23) (1997) 4613–4616.
- [24] M. Soccio, A. Nogales, N. Lotti, A. Munari, T.A. Ezquerro, Evidence of early stage precursors of polymer crystals by dielectric spectroscopy, *Phys. Rev. Lett.* 98 (3) (2007) 037801.
- [25] N.J. Terrill, P.A. Fairclough, E. Towns-Andrews, B.U. Komanschek, R.J. Young, A.J. Ryan, Density fluctuations: the nucleation event in isotactic polypropylene crystallization, *Polymer* 39 (11) (1998) 2381–2385.
- [26] K. Kaji, K. Nishida, T. Kanaya, G. Matsuba, T. Konishi, M. Imai, Spinodal crystallization of polymers: Crystallization from the unstable melt, *Adv. Polym. Sci.* 191 (2005) 187–240.
- [27] S. Sasaki, K. Tashiro, M. Kobayashi, Y. Izumi, K. Kobayashi, Microscopically viewed structural change of PE during the isothermal crystallization from the melt: II. Conformational ordering and lamellar formation mechanism derived from the coupled interpretation of time-resolved SAXS and FTIR data, *Polymer* 40 (25) (1999) 7125–7135.
- [28] P.D. Olmsted, W.C. Poon, T. McLeish, N. Terrill, A. Ryan, Spinodal-assisted crystallization in polymer melts, *Phys. Rev. Lett.* 81 (2) (1998) 373.
- [29] Z.-G. Wang, B.S. Hsiao, E.B. Sirota, P. Agarwal, S. Srinivas, Probing the early stages of melt crystallization in polypropylene by simultaneous small-angle X-ray scattering and laser light scattering, *Macromolecules* 33 (3) (2000) 978–989.
- [30] C. Liu, M. Muthukumar, Langevin dynamics simulations of early-stage polymer nucleation and crystallization, *J. Chem. Phys.* 109 (6) (1998) 2536–2542.
- [31] P. Welch, M. Muthukumar, Molecular mechanisms of polymer crystallization from solution, *Phys. Rev. Lett.* 87 (21) (2001) 218302.
- [32] M. Muthukumar, Molecular modelling of nucleation in polymers, *Philos. Trans. R. Soc. Lond. Ser. A Math. Phys. Eng. Sci.* 361 (1804) (2003) 539–556.
- [33] R.H. Gee, N. Lacevic, L.E. Fried, Atomistic simulations of spinodal phase separation preceding polymer crystallization, *Nature Mater.* 5 (1) (2006) 39–43.
- [34] P. Panine, E. Di Cola, M. Sztucki, T. Narayanan, Early stages of polymer melt crystallization, *Polymer* 49 (3) (2008) 676–680.
- [35] G. Strobl, Colloquium: Laws controlling crystallization and melting in bulk polymers, *Rev. Modern Phys.* 81 (3) (2009) 1287–1300.
- [36] C. Luo, J.-U. Sommer, Growth pathway and precursor states in single lamellar crystallization: MD simulations, *Macromolecules* 44 (6) (2011) 1523–1529.
- [37] Y.-l. Hong, S. Yuan, Z. Li, Y. Ke, K. Nozaki, T. Miyoshi, Three-dimensional conformation of folded polymers in single crystals, *Phys. Rev. Lett.* 115 (16) (2015) 168301.
- [38] S. Yuan, Z. Li, Y.-l. Hong, Y. Ke, J. Kang, A. Kamimura, A. Otsubo, T. Miyoshi, Folding of polymer chains in the early stage of crystallization, *ACS Macro Lett.* 4 (12) (2015) 1382–1385.
- [39] W.-T. Chuang, W.-B. Su, U.-S. Jeng, P.-D. Hong, C.-J. Su, C.-H. Su, Y.-C. Huang, K.-F. Laio, A.-C. Su, Formation of mesomorphic domains and subsequent structural evolution during cold crystallization of poly (trimethylene terephthalate), *Macromolecules* 44 (5) (2011) 1140–1148.
- [40] J.-B. Jheng, W.-T. Chuang, P.-D. Hong, Y.-C. Huang, U.-S. Jeng, C.-J. Su, G.-R. Pan, Formation of mesomorphic domains associated with dimer aggregates of phenyl rings in cold crystallization of poly (trimethylene terephthalate), *Polymer* 54 (22) (2013) 6242–6252.
- [41] T. Konishi, W. Sakatsuji, K. Fukao, Y. Miyamoto, Polymer crystallization mechanism through a mesomorphic state, *Phys. Rev. B* 84 (13) (2011) 132102.
- [42] T. Konishi, W. Sakatsuji, K. Fukao, Y. Miyamoto, Temperature dependence of lamellar thickness in isothermally crystallized poly (butylene terephthalate), *Macromolecules* 49 (6) (2016) 2272–2280.
- [43] T. Konishi, W. Sakatsuji, Y. Miyamoto, Crystallization through mesophase in poly (butylene terephthalate): Approach from dependence of growth rate on lamellar thickness, *Polymer* 119 (2017) 160–166.
- [44] D. Tadokoro, T. Konishi, K. Fukao, Y. Miyamoto, Lamellar crystallization of poly (trimethylene terephthalate), *Polym. J.* 55 (2) (2023) 775–783.

- [45] A. Keller, M. Hikosaka, S. Rastogi, A. Toda, P. Barham, G. Goldbeck-Wood, An approach to the formation and growth of new phases with application to polymer crystallization: effect of finite size, metastability, and ostwald's rule of stages, *J. Mater. Sci.* 29 (1994) 2579–2604.
- [46] G. Strobl, From the melt via mesomorphic and granular crystalline layers to lamellar crystallites: A major route followed in polymer crystallization? *Eur. Phys. J. E* 3 (2000) 165–183.
- [47] G. Strobl, A thermodynamic multiphase scheme treating polymer crystallization and melting, *Eur. Phys. J. E* 18 (2005) 295–309.
- [48] T. Konishi, D. Okamoto, D. Tadokoro, Y. Kawahara, K. Fukao, Y. Miyamoto, Origin of SAXS intensity in the low-q region during the early stage of polymer crystallization from both the melt and glassy state, *Phys. Rev. Mater.* 2 (10) (2018) 105602.
- [49] T. Konishi, D. Okamoto, D. Tadokoro, Y. Kawahara, K. Fukao, Y. Miyamoto, Kinetics of polymer crystallization with aggregating small crystallites, *Phys. Rev. Lett.* 128 (10) (2022) 107801.
- [50] T. Konishi, K. Taguchi, K. Fukao, N. Takagi, Y. Miyamoto, Crystallization with nodular aggregation near the glass transition temperature for syndiotactic polypropylene, *ACS Macro Lett.* 12 (2) (2023) 208–214.
- [51] Y. Chonan, G. Matsuba, K. Nishida, W. Hu, Crystal morphology of polyurea on rapid quenching, *Polymer* 213 (2021) 123201.
- [52] A.N. Kolmogorov, On the statistical theory of crystallization of metals [in Russian], *Izv. Akad. Nauk. SSSR Ser. Mat.* 3 (1937) 355–360.
- [53] J. William, R. Mehl, Reaction kinetics in processes of nucleation and growth, *Trans. Metall. Soc. AIME* 135 (1939) 416–442.
- [54] M. Avrami, Kinetics of phase change. I general theory, *J. Chem. Phys.* 7 (12) (1939) 1103–1112.
- [55] M. Avrami, Kinetics of phase change. II transformation-time relations for random distribution of nuclei, *J. Chem. Phys.* 8 (2) (1940) 212–224.
- [56] M. Avrami, Granulation, phase change, and microstructure kinetics of phase change. III, *J. Chem. Phys.* 9 (2) (1941) 177–184.
- [57] K. Sekimoto, Evolution of the domain structure during the nucleation-and-growth process with non-conserved order parameter, *Phys. A* 135 (2–3) (1986) 328–346.
- [58] F. Frank, Nucleation-controlled growth on a one-dimensional growth of finite length, *J. Cryst. Growth* 22 (3) (1974) 233–236.
- [59] J. Rault, Process of crystallization of polymers at low supercooling, *J. Phys. Lett.* 39 (21) (1978) 411–413.
- [60] M. Hikosaka, T. Seto, Growth rate of polyethylene single crystals at high pressure, *Japan. J. Appl. Phys.* 23 (8) (1984) 956.
- [61] M. Hikosaka, Unified theory of nucleation of folded-chain crystals and extended-chain crystals of linear-chain polymers, *Polymer* 28 (8) (1987) 1257–1264.
- [62] S. Rastogi, M. Hikosaka, H. Kawabata, A. Keller, Role of mobile phases in the crystallization of polyethylene. Part 1. Metastability and lateral growth, *Macromolecules* 24 (24) (1991) 6384–6391.
- [63] T. Cho, W. Stille, G. Strobl, Zero growth temperature of crystallizing polyethylene, *Macromolecules* 40 (7) (2007) 2596–2599.
- [64] T. Hugel, G. Strobl, R. Thomann, Building lamellae from blocks: the pathway followed in the formation of crystallites of syndiotactic polypropylene, *Acta Polymerica* 50 (5–6) (1999) 214–217.
- [65] B. Heck, T. Hugel, M. Iijima, E. Sadiku, G. Strobl, Steps in the transition of an entangled polymer melt to the partially crystalline state, *New J. Phys.* 1 (1) (1999) 17.
- [66] T.-Y. Cho, W. Stille, G. Strobl, Zero growth temperature and growth kinetics of crystallizing poly (*e*-caprolactone), *Colloid Polym. Sci.* 285 (8) (2007) 931–934.
- [67] G. Strobl, T. Cho, Growth kinetics of polymer crystals in bulk, *Eur. Phys. J. E* 23 (2007) 55–65.
- [68] M. Al-Hussein, G. Strobl, The melting line, the crystallization line, and the equilibrium melting temperature of isotactic polystyrene, *Macromolecules* 35 (5) (2002) 1672–1676.
- [69] T.-Y. Cho, G. Strobl, Temperature dependent variations in the lamellar structure of poly (l-lactide), *Polymer* 47 (4) (2006) 1036–1043.
- [70] T. Konishi, K. Nishida, G. Matsuba, T. Kanaya, Mesomorphic phase of poly (butylene-2, 6-naphthalate), *Macromolecules* 41 (9) (2008) 3157–3161.
- [71] D. Cavallo, D. Mileva, G. Portale, L. Zhang, L. Balzano, G.C. Alfonso, R. Androsch, Mesophase-mediated crystallization of poly (butylene-2, 6-naphthalate): an example of Ostwald's rule of stages, *ACS Macro Lett.* 1 (8) (2012) 1051–1055.
- [72] T. Konishi, Y. Miyamoto, Smectic structure and glass transition in poly (butylene terephthalate), *Polym. J.* 42 (4) (2010) 349–353.
- [73] P. Supaphol, J. Spruiell, Isothermal melt-and cold-crystallization kinetics and subsequent melting behavior in syndiotactic polypropylene: a differential scanning calorimetry study, *Polymer* 42 (2) (2001) 699–712.
- [74] S. Poulin-Dandurand, S. Pérez, J.-F. Revol, F. Brisse, The crystal structure of poly (trimethylene terephthalate) by X-ray and electron diffraction, *Polymer* 20 (4) (1979) 419–426.
- [75] T. Nakaoki, Y. Ohira, H. Hayashi, F. Horii, Spontaneous crystallization of the planar zigzag form of syndiotactic polypropylene at 0° C, *Macromolecules* 31 (8) (1998) 2705–2706.
- [76] Y. Ohira, F. Horii, T. Nakaoki, Spontaneous crystallization process of the planar zigzag form at 0 C from the melt for syndiotactic polypropylene, *Macromolecules* 33 (5) (2000) 1801–1806.
- [77] T. Nakaoki, T. Yamanaka, Y. Ohira, F. Horii, Dynamic FT-IR analysis of the crystallization to the planar zigzag form for syndiotactic polypropylene, *Macromolecules* 33 (7) (2000) 2718–2721.
- [78] Y. Ohira, F. Horii, T. Nakaoki, Crystal transformation behavior and structural changes of the planar zigzag form for syndiotactic polypropylene, *Macromolecules* 33 (15) (2000) 5566–5573.
- [79] Y. Ohira, F. Horii, T. Nakaoki, Conformational changes of the noncrystalline chains for syndiotactic polypropylene as a function of temperature: correlations with the crystallizations of form I and form III, *Macromolecules* 34 (6) (2001) 1655–1662.
- [80] T. Nakaoki, Y. Ohira, F. Horii, Investigation of the crystallization process of syndiotactic polypropylene quenched at 0° C from the melt or concentrated solutions by solid-state ¹³C NMR spectroscopy, *Polymer* 42 (10) (2001) 4555–4561.
- [81] Vittoria, L. Guadagno, A. Comotti, R. Simonutti, F. Auriemma, C. De Rosa, Mesomorphic form of syndiotactic polypropylene, *Macromolecules* 33 (16) (2000) 6200–6204.
- [82] C. De Rosa, O.R. de Ballesteros, M. Santoro, F. Auriemma, Influence of the quenching temperature on the crystallization of the trans-planar mesomorphic form of syndiotactic polypropylene, *Polymer* 44 (20) (2003) 6267–6272.
- [83] C. De Rosa, F. Auriemma, O.R. de Ballesteros, Influence of the stereoregularity on the crystallization of the trans planar mesomorphic form of syndiotactic polypropylene, *Polymer* 42 (24) (2001) 9729–9734.
- [84] L. Guadagno, C. D'Aniello, C. Naddeo, Vittoria, S.V. Meille, Elasticity of the oriented mesomorphic form of syndiotactic polypropylene, *Macromolecules* 35 (10) (2002) 3921–3927.
- [85] P. Corradini, G. Natta, P. Ganis, P. Temussi, Crystal structure of syndiotactic polypropylene, *J. Polym. Sci. C: Polym. Symposia* 16 (5) (1967) 2477–2484.
- [86] B. Lotz, A.J. Lovinger, R.E. Cais, Crystal structure and morphology of syndiotactic polypropylene single crystals, *Macromolecules* 21 (8) (1988) 2375–2382.
- [87] C. De Rosa, F. Auriemma, Structure and physical properties of syndiotactic polypropylene: A highly crystalline thermoplastic elastomer, *Progr. Polym. Sci.* 31 (2) (2006) 145–237.
- [88] J.K. Percus, G.J. Yevick, Analysis of classical statistical mechanics by means of collective coordinates, *Phys. Rev.* 110 (1) (1958) 1.
- [89] D. Thomas, L. Staveley, 889. A study of the supercooling of drops of some molecular liquids, *J. Chem. Soc. (Resumed)* 889 (1952) 4569–4577.
- [90] J.D. Hoffman, R.L. Miller, H. Marand, D.B. Roitman, Relationship between the lateral surface free energy. sigma. and the chain structure of melt-crystallized polymers, *Macromolecules* 25 (8) (1992) 2221–2229.
- [91] A. Toda, Y. Furushima, C. Schick, Crystal domains and crystallization kinetics of poly (butylene terephthalate), *Macromolecules* 56 (17) (2023) 6891–6902.
- [92] N. Grozev, I. Botiz, G. Reiter, Morphological instabilities of polymer crystals, *Eur. Phys. J. E* 27 (2008) 63–71.
- [93] B. Zhang, J. Chen, H. Zhang, M.C. Baier, S. Mecking, R. Reiter, R. Mülhaupt, G. Reiter, Annealing-induced periodic patterns in solution grown polymer single crystals, *RSC Adv.* 5 (17) (2015) 12974–12980.
- [94] K. Taguchi, Y. Miyamoto, A. Toda, Molecular weight dependence of crystal growth in isotactic polystyrene ultrathin films, *ACS Macro Lett.* 8 (10) (2019) 1227–1232.
- [95] Y. Wang, B. Chen, K.E. Evans, O. Ghita, Novel fibre-like crystals in thin films of Poly Ether Ether Ketone (PEEK), *Mater. Lett.* 184 (2016) 112–118.
- [96] Y. Wang, B. Chen, K. Evans, O. Ghita, Enhanced ductility of PEEK thin film with self-assembled fibre-like crystals, *Sci. Rep.* 8 (1) (2018) 1314.
- [97] K. Schätzel, B.J. Ackerson, Density fluctuations during crystallization of colloids, *Phys. Rev. E* 48 (5) (1993) 3766.
- [98] P.R. ten Wolde, D. Frenkel, Enhancement of protein crystal nucleation by critical density fluctuations, *Science* 277 (5334) (1997) 1975–1978.
- [99] U. Gasser, E.R. Weeks, A. Schofield, P. Pusey, D. Weitz, Real-space imaging of nucleation and growth in colloidal crystallization, *Science* 292 (5515) (2001) 258–262.
- [100] H.J. Schöpe, G. Bryant, W. Van Megen, Two-step crystallization kinetics in colloidal hard-sphere systems, *Phys. Rev. Lett.* 96 (17) (2006) 175701.
- [101] J. Savage, A. Dinsmore, Experimental evidence for two-step nucleation in colloidal crystallization, *Phys. Rev. Lett.* 102 (19) (2009) 198302.
- [102] A. Sanz, A. Nogales, I. Puente-Orench, M. Jiménez-Ruiz, T.A. Ezquerro, Detection of early stage precursor during formation of plastic crystal ethanol from the supercooled liquid state: a simultaneous dielectric spectroscopy with neutron diffraction study, *Phys. Rev. Lett.* 107 (2) (2011) 025502.
- [103] T. Schilling, H.J. Schöpe, M. Oettel, G. Opletal, I. Snook, Precursor-mediated crystallization process in suspensions of hard spheres, *Phys. Rev. Lett.* 105 (2) (2010) 025701.
- [104] J. Russo, H. Tanaka, The microscopic pathway to crystallization in supercooled liquids, *Sci. Rep.* 2 (1) (2012) 505.
- [105] J.F. Lutsko, G. Nocolis, Theoretical evidence for a dense fluid precursor to crystallization, *Phys. Rev. Lett.* 96 (4) (2006) 046102.
- [106] J.F. Lutsko, A dynamical theory of nucleation for colloids and macromolecules, *J. Chem. Phys.* 136 (3) (2012).
- [107] T. Kawasaki, H. Tanaka, Formation of a crystal nucleus from liquid, *Proc. Natl. Acad. Sci.* 107 (32) (2010) 14036–14041.



Takashi Konishi has worked as an assistant professor at the Graduate School of Human and Environmental Studies, Kyoto University from 2008. He obtained his Ph.D. in Graduate School of Engineering, Kyoto University in 2006 under the supervisor Prof. T. Kanaya. Thereafter, he studied soft matter physics with Prof. H. Tanaka at Institute of Industrial Science, The University of Tokyo, as a postdoctoral researcher from 2006 to 2008. His current of research interests include the mechanism of polymer crystallization and the structural changes in elastomers.



Yoshihisa Miyamoto obtained a Ph.D. in Physics at the Graduate School of Science, Kyoto University in 1983 under the supervision of Prof. K. Asai. He worked as an assistant(1984–1990), an assistant professor(1990–2003) at the College of Liberal Arts and Sciences, and a professor(2003–2018) at the Graduate School of Human and Environmental Studies, Kyoto University. His current fields of research interests include the kinetics and morphology in polymer crystallization and the memory effects in glass.